International Journal of Thermal Sciences 48 (2009) 1814–1822

Contents lists available at ScienceDirect

International Journal of Thermal Sciences

journal homepage: www.elsevier.com/locate/ijts

Study of dimethyl ether homogeneous charge compression ignition combustion process using a multi-dimensional computational fluid dynamics model

Chen Huang [a,*], Mingfa Yao [b], Xingcai Lu [a], Zhen Huang [a]

[a] Key Laboratory for Power Machinery and Engineering of M.O.E., Shanghai Jiaotong University, Shanghai, PR China
[b] State Key Laboratory of Engine Combustion, Tianjin University, Tianjin, PR China

ARTICLE INFO

Article history:
Received 25 December 2007
Received in revised form
31 October 2008
Accepted 5 February 2009
Available online 18 March 2009

Keywords:
Homogeneous Charge Compression Ignition
Dimethyl Ether
Reduced Chemical Mechanism
Multi-dimensional CFD Model
Emissions

ABSTRACT

A multi-dimensional Computational Fluid Dynamics (CFD) model is adopted to investigate the Dimethyl Ether (DME) Homogeneous Charge Compression Ignition (HCCI) combustion and emissions processes. A reduced chemical mechanism is coupled with a CFD code in the multi-dimensional CFD model. The pressure profiles predicted by the multi-dimensional CFD model are more accurate than the single-zone model, because the wall heat transfer and in-cylinder turbulence flow are considered. During the combustion process the in-cylinder temperature distribution undergoes a process from inhomogeneity to homogeneity. Both low and high temperature reactions don't occur simultaneously throughout the cylinder. The low temperature reactions are initiated near the piston surface and squish region, and the high temperature reactions are initiated in the combustion chamber core zone and squish region. Emission analysis indicates that unburned fuel and CH_2O account for the majority of unburned hydrocarbon (HC). The unburned fuel, CH_2O and CO emission mainly resides in the bottom, middle and upper part of the piston-ring crevice region, respectively. With the decrease of DME equivalence ratio, unburned fuel and CO increases. However, when the DME equivalence ratio is too small, CO emission decreases.

1. Introduction

With ever growing concerns on environmental pollution, energy security, and future oil supplies, the global community is seeking nonpetroleum based alternative fuels, along with more advanced combustion technology (e.g., Homogeneous Charge Compression Ignition) to increase the efficiency of energy use [1].

Homogeneous Charge Compression Ignition (HCCI) is a promising combustion mode that can achieve high efficiency and low emissions simultaneously, and it is also a key strategy to meet future emission regulations. However, there are still challenges associated with the attracting features of HCCI combustion. For one thing, it's hard to control the combustion phasing over a wide range of operation conditions. For another thing, the unburned hydrocarbon (HC) and carbon monoxide (CO) emissions are comparatively higher than traditional diesel engine. Besides, fundamental understanding of the HCCI combustion and emissions processes is still limited [2,3].

Dimethyl ether (DME) has the potential to be a clean and efficient alternative fuel for diesel [4]. This is not only because of its high cetane number (above 55), low auto-ignition temperature and low boiling point (−25 °C), but also because of its simple chemical structure and high oxygen content which result in soot-free combustion in engines. In addition, DME can be produced by the conversion of various feedstocks such as natural gas, coal, oil residues and bio-mass, and it reduces the dependence of petroleum fuels which are depleting [5].

DME has been attracting much attention not only as an alternative fuel but also as an ignition promoter when it's implemented into HCCI combustion system. Shudo et al. [6,7] proposed a HCCI combustion system fueled with DME and methanol-reformed gas (MRG). In the system, both DME and MRG were produced from methanol by onboard reformers utilizing exhaust heat from the engine. The research showed high thermal efficiency and the operable range was expanded with the two kinds of fuel. Sato et al. [8] adjusted the DME proportion to control the HCCI combustion process for DME/methane dual-fueled HCCI engine. Yamada et al. [9] reported the reduction of the first stage heat release with methanol addition and consequent retardation of the second stage heat release in a DME HCCI engine. Flowers et al. [10] used chemical kinetics code to analyze the natural gas HCCI combustion process, and DME addition was adopted as a control strategy. Yao et al. [11,12] applied DME as an ignition improver for both Compressed Natural Gas (CNG) and Methanol HCCI combustion processes.

* Corresponding author. Tel.: +86 21 34206859; fax: +86 21 34205553.
E-mail address: hubbub@sjtu.edu.cn (C. Huang).

1290-0729/$ – see front matter © 2009 Elsevier Masson SAS. All rights reserved.
doi:10.1016/j.ijthermalsci.2009.02.006

With the rapid development of combustion modeling theory and computational technology, engine combustion simulation has become a useful tool in understanding in-cylinder details and engine design guidance. Although HCCI combustion is controlled primarily by chemical kinetics, there is still mixture and temperature inhomogeneity due to wall heat transfer and turbulence interaction. Thus, there are three categories of models for HCCI combustion simulation: single-zone model, multi-zone model and multi-dimensional CFD

Table 1
The reduced chemical mechanism for DME.

Species				
CH_3OCH_2	$CH_3OCH_2O_2$	$CH_2OCH_2O_2H$	$CH_3OCH_2O_2H$	CH_3OCH_3
H	CH_3O	CH_3	O_2	OH
H_2O	N_2	CO	HCO	CO_2
HO_2	H_2O_2	CH_2OH	CH_2O	HCO_2
OCH_2OCHO	HO_2CH_2OCHO	$O_2CH_2OCH_2O_2H$	H_2	CH_3OCH_2O
O				
	Reactions (k = AT**b exp(−E/RT))	A	b	E
1	$CH_3OCH_3 + OH = CH_3OCH_2 + H_2O$	1.40E + 08	1.6	−35.0
2	$CH_3OCH_2O_2 = CH_3OCH_2 + O_2$	4.68E + 17	−1.2	38 240.0
	Reverse Arrhenius coefficients:	1.00E + 12	0.0	0.0
3	$CH_3OCH_2O_2 = CH_2OCH_2O_2H$	7.42E + 11	0.0	18 500.0
	Reverse Arrhenius coefficients:	3.10E + 13	−0.8	9340.0
4	$O_2CH_2OCH_2O_2H = CH_2OCH_2O_2H + O_2$	4.99E + 17	−1.2	38 260.0
	Reverse Arrhenius coefficients:	9.00E + 11	0.0	0.0
5	$O_2CH_2OCH_2O_2H = HO_2CH_2OCHO + OH$	3.71E + 11	0.0	18 500.0
6	$HO_2CH_2OCHO = OCH_2OCHO + OH$	1.01E + 20	−1.5	44 090.0
7	$OCH_2OCHO = CH_2O + HCO_2$	5.05E + 16	−1.6	15 400.0
	Reverse Arrhenius coefficients:	1.25E + 11	0.0	7400.0
8	$OH + OH(+M) = H_2O_2(+M)$	1.24E + 14	−0.4	0.0
	Low pressure limit:	0.30410E + 31	−0.46300E + 01	0.20490E + 04
	TROE centering: 0.47000E + 00	0.10000E + 03	0.20000E + 04	0.10000E + 16
	H_2 Enhanced by 2.000E + 00			
	H_2O Enhanced by 1.200E + 01			
	CO Enhanced by 1.900E + 00			
	CO_2 Enhanced by 3.800E + 00			
9	$H_2O_2 + O_2 = HO_2 + HO_2$	2.96E + 12	0.0	38 150.0
	Reverse Arrhenius coefficients:	4.20E + 14	0.0	11 980.0
	Declared duplicate reaction…			
10	$H_2O_2 + O_2 = HO_2 + HO_2$	0.00E + 00	0.0	38 150.0
	Reverse Arrhenius coefficients:	1.30E + 11	0.0	−1629.0
	Declared duplicate reaction…			
11	$CH_2OCH_2O_2H = OH + CH_2O + CH_2O$	1.25E + 13	0.0	18 160.0
	Reverse Arrhenius coefficients:	0.00E + 00	0.0	0.0
12	$CH_2O + OH = HCO + H_2O$	3.43E + 09	1.2	−447.0
	Reverse Arrhenius coefficients:	2.35E + 08	1.4	26 120.0
13	$HCO + O_2 = CO + HO_2$	9.10E + 12	0.0	410.0
	Reverse Arrhenius coefficients:	1.69E + 14	−0.3	34 590.0
14	$CO + OH = CO_2 + H$	9.42E + 03	2.3	−2351.0
	Reverse Arrhenius coefficients:	1.06E + 06	2.3	19 980.0
15	$CH_3OCH_3 + O_2 = CH_3OCH_2 + HO_2$	4.10E + 13	0.0	44 910.0
	Reverse Arrhenius coefficients:	1.90E + 11	0.0	−4659.0
16	$HO_2 + M = H + O_2 + M$	3.57E + 24	−2.7	51 620.0
	Reverse Arrhenius coefficients:	6.70E + 19	−1.4	0.0
17	$CO + HO_2 = CO_2 + OH$	1.51E + 14	0.0	23 650.0
	Reverse Arrhenius coefficients:	3.23E + 16	−0.3	85 260.0
18	$CH_3 + HO_2 = CH_3O + OH$	1.50E + 13	0.0	0.0
	Reverse Arrhenius coefficients:	6.52E + 14	−0.3	24 550.0
19	$CH_3OCH_2O_2H = CH_3OCH_2O + OH$	1.83E + 20	−1.5	47 160.0
	Reverse Arrhenius coefficients:	2.00E + 13	0.0	0.0
20	$CH_3OCH_3 + HO_2 = CH_3OCH_2 + H_2O_2$	1.00E + 13	0.0	17 690.0
	Reverse Arrhenius coefficients:	6.54E + 13	−0.6	9290.0
21	$CH_3OCH_2O = CH_3O + CH_2O$	6.48E + 12	−0.1	14 870.0
	Reverse Arrhenius coefficients:	1.25E + 11	0.0	7400.0
22	$CH_2OH + O_2 = CH_2O + HO_2$	1.00E + 14	0.0	5000.0
	Reverse Arrhenius coefficients:	3.26E + 12	0.6	25 860.0
23	$CH_2O + O = HCO + OH$	4.16E + 11	0.6	2762.0
	Reverse Arrhenius coefficients:	1.46E + 10	0.6	15 340.0
24	$CH_2O + HO_2 = HCO + H_2O_2$	5.60E + 12	0.0	13 600.0
	Reverse Arrhenius coefficients:	7.79E + 11	0.0	10230.0
25	$HCO + HO_2 = CH_2O + O_2$	1.00E + 14	0.0	3000.0
	Reverse Arrhenius coefficients:	3.66E + 15	0.0	46 040.0
26	$HCO_2 + M = H + CO_2 + M$	2.29E + 26	−3.0	35 070.0
	Reverse Arrhenius coefficients:	5.95E + 24	−2.6	37 850.0
27	$CH_2OH + M = CH_2O + H + M$	1.85E + 24	−2.5	34 190.0
	Reverse Arrhenius coefficients:	1.06E + 23	−2.0	5901.0
28	$H_2O + M = H + OH + M$	1.84E + 27	−3.0	122 600.0
	Reverse Arrhenius coefficients:	2.25E + 22	−2.0	0.0

NOTE: A units mole cm sec K, E units cal/mole.

Table 2
Engine specifications.

Bore	115 mm
Stroke	115 mm
Displacement	1200 cm^3
Compression Ratio	17.0:1
Engine Speed	1400 r/min
Intake Valve Open	12°BTDC
Intake Valve Close	45°ABDC
Exhaust Valve Open	55°BBDC
Exhaust Valve Close	14°ATDC

model. The feasibility of each model varies and the user needs to compromise between computer time and model accuracy [13].

The single-zone model is the simplest HCCI simulation model. This model is based on the assumption that the in-cylinder mixture is perfectly homogeneous which leads to a rapid fuel consumption and heat release [14]. Chemical mechanism is the center of a single-zone model, and it's also the fundamental and preliminary work for the multi-zone and multi-dimensional CFD models. Various kinds of chemical mechanisms describing DME HCCI combustion process have been developed over recent years. Curran et al. [15,16] proposed a detailed DME oxidation mechanism which included 79 species and 351 reactions. This comprehensive mechanism was validated against a series of experimental results over a wide range of conditions. However, the use of detailed chemical mechanism with the multi-dimensional CFD code is too computationally intensive for current computer. Thus, reduced chemical mechanisms which are accurate in predicting fuel oxidation process under engine operating conditions are paid much attention. Yamada et al. [17] developed a reduced chemical mechanism of DME consisting of 23 species and 23 reactions. Satisfactory agreement with detailed mechanism was obtained, and the effects of formaldehyde and methanol as ignition suppressors were studied. Kim et al. [18] also established a reduced chemical mechanism of DME including 28 species and 45 reactions. The key reactions of DME affecting the ignition delay in Negative Temperature Coefficient (NTC) were investigated. By analyzing the detailed DME oxidization pathway, Yao et al. [19,20] proposed a reduced chemical mechanism consisting of 28 reactions and 26 species.

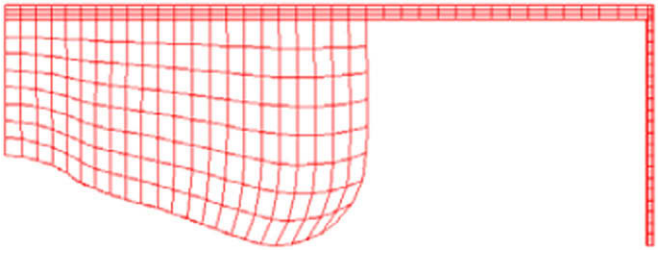

Fig. 1. Computational mesh of combustion chamber at TDC.

The second type of HCCI combustion simulation model is the multi-zone model, which is a little more complicated than the single-zone model. The combustion chamber is divided into a certain number of zones to account for the mixture and temperature inhomogeneity [14]. Thus, different levels of mixture and temperature stratifications which exist in actual HCCI combustion process are considered. The multi-zone model can predict a reasonable overall combustion rate but it requires empirical adjustments in formulating zones [13]. Aceves et al. [21,22] focused on developing and validating multi-zone models for HCCI combustion to obtain some of the zonal resolution afforded by CFD models. In their previous version of multi-zone model, the fluid mechanics code KIVA was run to evaluate the temperature distribution inside the cylinder before combustion, and the information was then fed into the chemical kinetic code. The results showed considerable success in predicting maximum pressure, burn duration, indicated efficiency and combustion efficiency, but HC and CO emissions were not as good. An upgraded version of the above multi-zone model was proposed by Babajimopoulos et al. [23] to study the Premixed Charge Compression Ignition (PCCI) combustion process. In this model KIVA-3 V was fully integrated with the multi-zone model and chemical kinetics. At each discrete time the cells were grouped into zones according to the temperature and composition of the cells. Each zone was treated as an adiabatic constant volume reactor, and was solved by CHEMKIN during the time step. Then the new zone composition and heat release were mapped back onto all the cells within the zones, and KIVA-3 V code subsequently proceeded to determine convection and diffusion processes over the same time step.

The last and the most comprehensive type of HCCI combustion model is the multi-dimensional CFD model. This model can analyze the effects of combustion chamber geometry, wall heat transfer and turbulence influence on HCCI combustion process and it can also be applied to other stratified mixture combustion simulations. A multi-dimensional CFD model coupled with detailed chemical kinetics was proposed by Kong et al. [3], and a formulation where the reaction rate for each species incorporating the effects of both chemical kinetics and turbulent mixing was included in the model. The model gave better prediction in ignition timing and combustion phasing. The HC emissions were well predicted, and the CO emissions were under predicted. However, by modifying a key oxidation reaction rate constant of CO reaction, the CO emission prediction was improved. Kong [13] further studied the HCCI combustion characteristics of

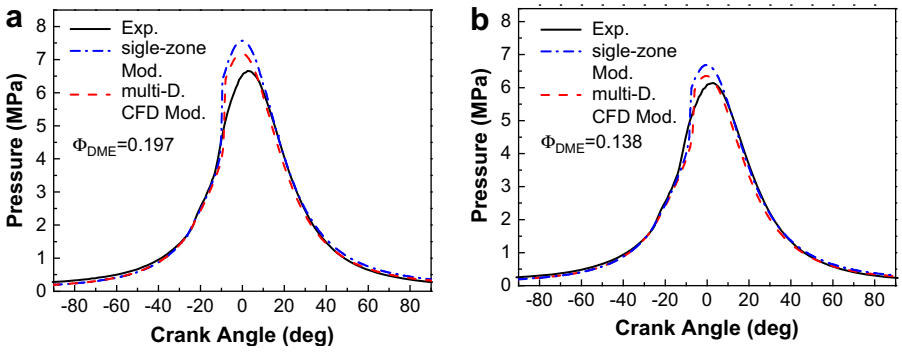

Fig. 2. Comparison of cylinder pressure profiles predicted by multi-dimensional CFD model, single-zone model and experimental results.

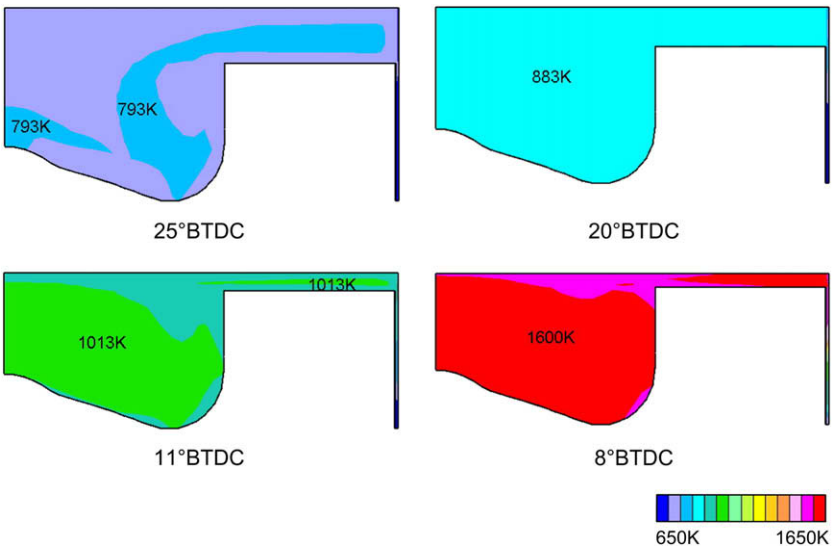

Fig. 3. The in-cylinder temperature distribution for DME HCCI combustion $\Phi_{DME} = 0.197$.

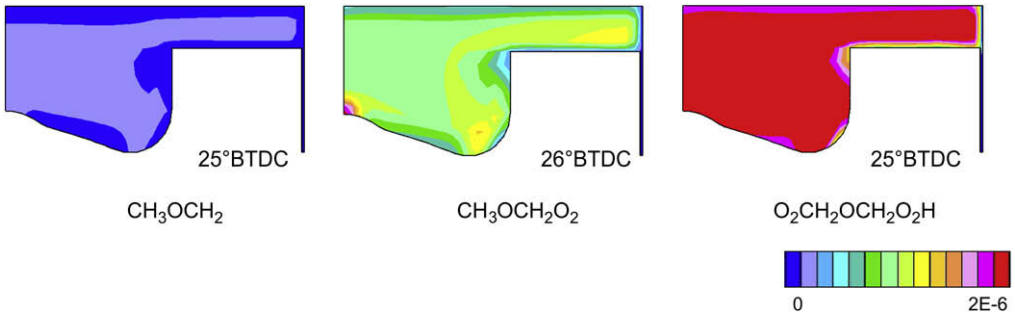

Fig. 4. The intermediate species mass fraction distribution at the beginning of LTR $\Phi_{DME} = 0.197$.

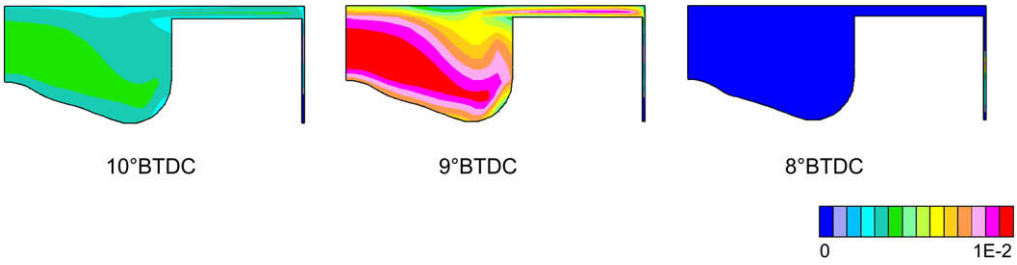

Fig. 5. CO mass fraction distribution $\Phi_{DME} = 0.197$.

natural gas and DME mixture with the multi-dimensional CFD model coupled with detailed chemistry. Combustion and operation limits were well predicted by the model. Although a coupled multi-dimensional CFD and detailed chemistry model can give accurate prediction of combustion characteristics, it requires substantial memory and CPU time. Thus, a reduced chemistry coupled with multi-dimensional CFD model is adopted to simulate the HCCI combustion process and emissions more efficiently. Noel et al. [24] reported the coupling between the reduced chemistry of n-heptane and CFD code to study the HCCI combustion process. Yao et al. [25] proposed a multi-dimensional CFD model coupled with reduced chemistry to study the DME/methanol dual-fuel HCCI combustion process and emissions.

In this study a reduced chemical mechanism is coupled with a multi-dimensional CFD code (STAR/Kinetics) to study the Dimethyl Ether HCCI combustion process and emissions. The multi-dimensional CFD model is more accurate in predicting the pressure profile than the single-zone model, because the wall heat transfer and in-cylinder turbulence flow are considered in the model. The HCCI combustion and emissions formation processes are analyzed, which have significant meanings to offer strategies to enable HCCI combustion.

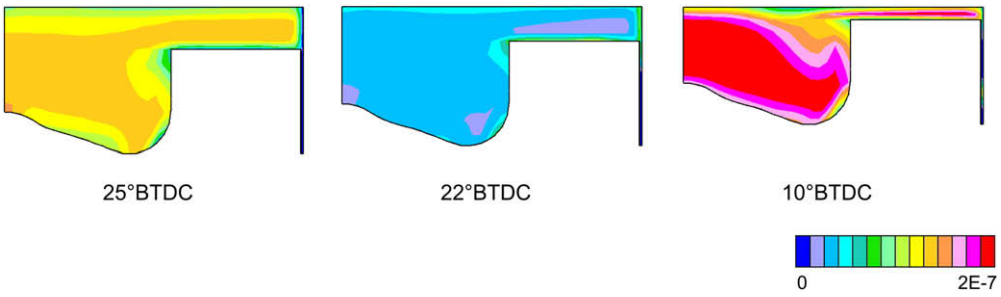

Fig. 6. OH mass fraction distribution $\Phi_{DME} = 0.197$.

2. Experiments

Experiments were conducted on a modified single-cylinder, water-cooled, direct-injection diesel engine. The engine specifications are shown in Table 2, and the detailed schematic diagram and operation condition is presented in the literature [12]. An electronically controlled fuel injection system was used for fueling DME. The DME injector was mounted near the inlet port of cylinder head, and it was controlled by an electromagnetic valve. Before the DME injector, there was a surge tube to stabilize the DME injection pressure to 0.25 MPa. The DME flow rate was calculated by calibration according to the injection pressure and duration. DME injection timing was at 20° After Top Dead Center (ATDC) in the intake stroke. A homogeneous mixture of DME with air was formed during the compression stroke.

The DME equivalence ratio is defined as follows,

$$\phi_{DME} = (G_{DME} \times AF_{DME})/G_{AIR} \quad (1)$$

where $G_{DME}$is the mass flow rate of DME and G_{AIR} is the mass flow rate of air. AF_{DME} represents the stoichiometric air/fuel ratio of DME.

3. Model formulation

3.1. Reduced chemical kinetics model for DME

A detailed chemistry coupled with CFD model is far beyond the capacity of current computer, thus a reduced chemistry which is specially developed for engine operation condition is preferable in this research. This paper adopted a reduced chemical mechanism for DME HCCI combustion process which was proposed by Yao et al. [17]. The reduced chemical mechanism has been derived from the detailed chemical mechanism [15,16] by analyzing the reaction pathways and sensitivity analysis. It consists of 26 species and 28 reactions, and the mechanism is shown in Table 1.

The reduced chemical mechanism has been validated against the detailed chemical mechanism at constant and variable volume simulations. First, the ignition delay calculated by the reduced mechanism is compared with the detailed mechanism under constant volume operation conditions. The initial temperature range is 600–1000 K, the initial pressure varies from 10 atm to 40 atm, and the DME equivalence ratio is 0.215. Second, the reduced chemical mechanism has been compared with the detailed chemical mechanism at HCCI engine operating conditions. Cylinder pressure, temperature and important intermediate species were compared with the detailed mechanism. Detailed description about the reduced mechanism is presented in this literature [17].

3.2. Multi-dimensional CFD model

The reduced chemical mechanism for DME has been implemented into the STAR/Kinetics CFD code to simulate HCCI combustion and emissions processes [26]. The STAR-CD code provides CHEMKIN the species and thermodynamic information of each computational cell, and the CHEMKIN code returns the new species information and energy release after solving the chemistry. The chemistry and flow solutions are then coupled. The turbulence affects the combustion by property transport, heat flux and mixture preparation [13].

The Renormalization Group (RNG) k–ε model was used for turbulence modeling. The Pressure-Implicit with Splitting of Operators (PISO) algorithm was used for the transient flow of the engine. PISO performs at each time step, a predictor, followed by a number of correctors, during which linear equation sets are solved iteratively for each main dependent variable. The decisions on the number of correctors and inner iterations are made internally on the basis of the splitting error and inner residual levels, respectively, according to prescribed tolerances and upper limits.

3.3. Initial conditions

The multi-dimensional CFD simulations were started at the time of intake valve close (IVC), and were ended at the time of exhaust valve open (EVO) assuming a uniform distribution of mixture properties. To reduce computational time, two simplifications were made. Firstly, one layer grid was applied, shown in Fig. 1. Secondly,

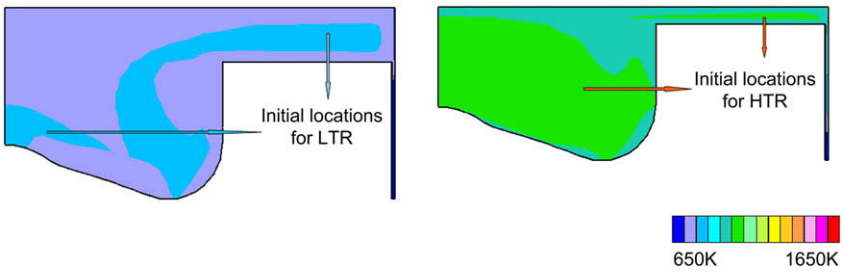

Fig. 7. Initial locations for LTR and HTR $\Phi_{DME} = 0.197$.

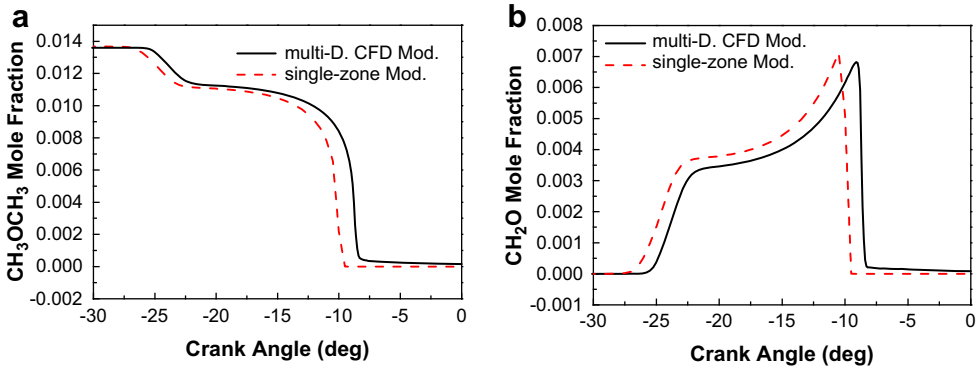

Fig. 8. History profiles of CH_3OCH_3 and CH_2O $\Phi_{DME} = 0.197$.

the coupling of turbulence flow and chemical kinetic model was activated at 30°BTDC, because the combustion reaction always takes place around top dead center (TDC). Engine speed was rated at 1400 rpm, and the time-varying parameters were converted into crank angle. There are 1658 cells at IVC, and the average cell size is about 2 mm. A full cycle simulation took approximately 18 h in a PC machine with Pentium IV 3.0 GHz CPU and 1 GB internal memory. For all the cases studied, the temperature and pressure at IVC were estimated as 375 K and 0.11 Mpa, respectively. The surface temperatures of the piston, cylinder head and liner were estimated as 500 K, 450 K and 420 K, respectively.

4. Results and discussions

4.1. Comparison of pressure profiles

Fig. 2 gives the comparison of cylinder pressure profiles predicted by the multi-dimensional CFD model, single-zone model and experimental results. The cylinder pressure profiles predicted by multi-dimensional CFD model are a little lower than those predicted by the single-zone model. On one side, the mixture inhomogeneity, wall heat transfer and in-cylinder turbulence flow are considered in the multi-dimensional CFD model, which results in lower pressure. On the other side, the turbulence reaction interaction (TCI) model is not considered in this multi-dimensional CFD model, and the turbulence has a small influence on the reaction rate. Thus, there is a slight difference in the pressure profiles predicted by the single-zone model and multi-dimensional CFD model. There are discrepancies in the pressure profiles between the multi-dimensional CFD model and the experimental data in Fig. 2. Two explanations might contribute to this result. On one hand, the simulation is performed on the assumption that the mixture is perfectly homogeneous at the beginning of calculation. However, the mixture and temperature inhomogeneity always exists in engine operating conditions. In other words, the fuel air mixture can hardly be mixed down to the molecular level experimentally. As a result, the heat release rate is slowed down and the peak pressure is decreased. On the other hand, the effect of turbulence on reaction rates are not considered in the sub-grid scale in this multi-dimensional CFD model, and the turbulence only affects the combustion by property transport and heat flux.

4.2. Analysis of combustion process

Theoretically, the mixture in HCCI combustion process is perfectly homogeneous, i.e. the temperature distribution and mixture concentration can be represented by spatially-averaged values. However, in actual HCCI combustion process there are still locations of temperature and mixture inhomogeneity due to mixture preparation, wall heat transfer and turbulence interaction.

Fig. 3 presents the cylinder temperature distribution simulated by the multi-dimensional CFD model. The DME equivalence ratio is

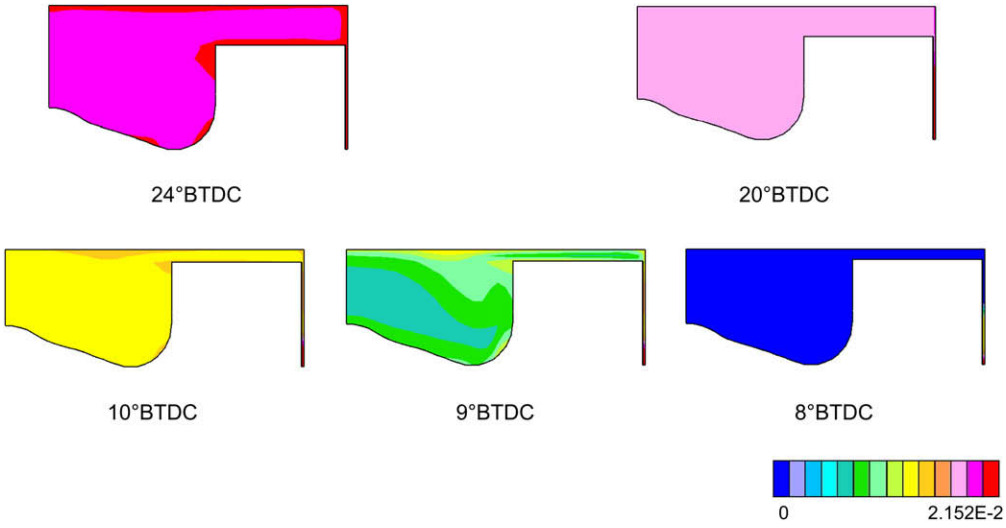

Fig. 9. CH_3OCH_3 mass fraction distribution $\Phi_{DME} = 0.197$.

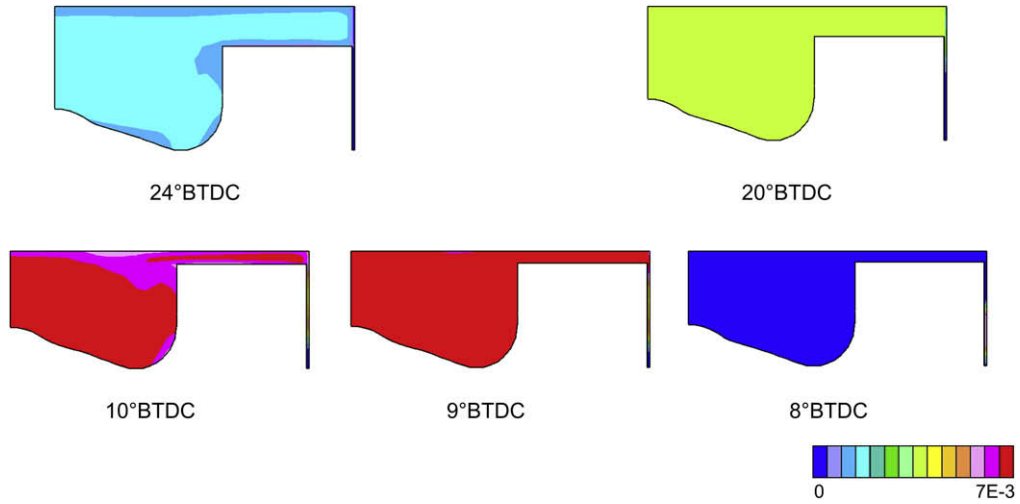

Fig. 10. CH_2O mass fraction distribution $\Phi_{DME} = 0.197$.

0.197. Low Temperature Reaction (LTR) of DME occurs in the temperature range 750–800 K. At the beginning of LTR, i.e. 25° Before Top Dead Center (BTDC), the temperature adjacent to the piston surface and squish region is slightly higher, which is 793 K. This is due to the in-cylinder turbulence flow. The mass fraction distributions of intermediate species during LTR are illustrated in Fig. 4. The concentrations of CH_3OCH_2, $CH_3OCH_2O_2$ and O_2CH_2O-CH_2O_2H are comparatively higher at the place near the piston surface and squish region, which means that the degenerate chain branching pathway, i.e. H-atom abstraction reaction R1, the first O_2 addition reaction R2 and the second O_2 addition reaction R4, proceeds more rapidly at those locations. The OH concentration at the beginning of LTR, i.e. 25°BTDC, also confirms the early heat release at those locations, shown in Fig. 6. Thus, it can be concluded that the initial locations for the LTR reside in the place adjacent to the piston surface and squish region, shown in Fig. 7. At the end of LTR, i.e. 20°BTDC, the temperature in the cylinder is more evenly distributed due to the low temperature heat release of DME, shown in Fig. 3. However, there are still different levels of temperature gradients near the cylinder wall and the piston-ring crevice region as a result of wall heat transfer. The OH mass concentration at 22°BTDC near the cylinder head is much higher, shown in Fig. 6, which indicates that the low temperature reactions move to the cylinder head. Multi-dimensional CFD simulation indicates that LTR for DME HCCI combustion process does not take place in the entire combustion chamber simultaneously. It occurs primarily at the place near the piston surface and the squish region, and subsequently moves to the place near cylinder head.

High Temperature Reaction (HTR) occurs when the cylinder temperature exceeding 1000 K. At the beginning of HTR, i.e. 11°BTDC, the temperature in the core and squish region is much higher, which are 1013 K, shown in Fig. 3. At the next crank angle, i.e. 10°BTDC, more CO and OH reside in the combustion chamber core zone and squish region, shown in Figs. 5 and 6. Thus, it can be concluded that the initial locations for HTR reside in the combustion chamber core zone and squish region, shown in Fig. 7. The temperature near the piston surface and the cylinder head is relatively lower, because much heat is lost through the cylinder head and piston surface, and the temperature gradients in those regions increase as the time elapses. At the end of HTR, i.e. 8°BTDC, the temperature distribution in the cylinder is rather uniform, and this is caused by the rapid heat release during the high temperature reaction region. Moreover, during the entire combustion process, the temperature in the piston-ring crevice region is much lower than the combustion chamber core zone, because much heat is lost from the piston-ring crevice region, where the emissions are most likely to appear.

Fig. 8 shows the history profiles of dimethyl ether and formaldehyde predicted by single-zone model and multi-dimensional CFD model, respectively. The consuming rate and producing rate predicted by multi-dimensional CFD model are a little slower than those predicted by single-zone model. Moreover, the dimethyl ether consuming timing predicted by the multi-dimensional CFD model is later than that predicted by the single-zone model. The reason is that in-cylinder turbulence flow and wall heat transfer are considered in the multi-dimensional CFD model.

Fig. 9 shows the dimethyl ether mass fraction distribution during the two-stage auto-ignition process. At the beginning of LTR, i.e. 24°BTDC, smaller amount of DME is remained in combustion chamber core and squish region, because these are the locations where LTR first takes place, shown in Fig. 7. At the end of LTR, i.e. 20°BTDC, there is still much DME residing in the cylinder, and the distribution is rather uniform. When HTR is dominate, i.e. 10°BTDC, DME concentration in the core and squish region is lower, because the temperature in those locations is higher than the rest of the cylinder. At the next crank angle, i.e. 9°BTDC, more DME in the core and squish region is consumed. However, the DME near the thermal boundary layer dose not disappear because of the wall heat transfer effect. At the end of HTR, i.e. 8°BTDC, the majority of DME is oxidized, and there is only a very small amount of DME left in the

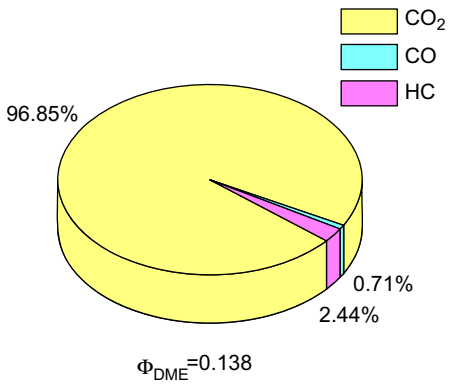

Fig. 11. The percentage of fuel carbon into emissions $\Phi_{DME} = 0.138$.

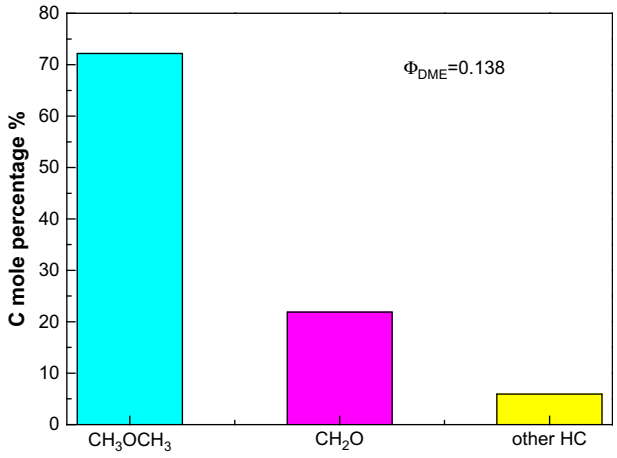

Fig. 12. Composition of unburned hydrocarbon $\Phi_{DME} = 0.138$.

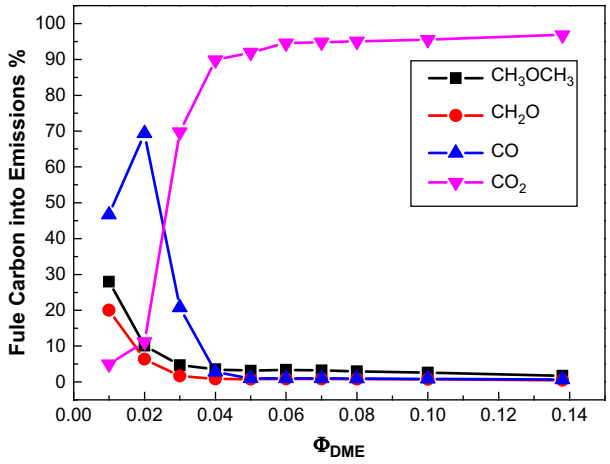

Fig. 14. The effect of DME equivalence ratio on the conversion ratio of fuel carbon into emissions.

piston-ring crevice region. Unburned fuel mainly comes from the piston-ring crevice region.

Formaldehyde is an important intermediate species during LTR and it's also a major component of HC emission. At the beginning of LTR, i.e. 24°BTDC, a small amount of CH_2O is formed in the combustion chamber core and squish region, shown in Fig. 10, which results in a slight temperature rise in those locations, shown in Fig. 3. Both single-zone model and multi-dimensional CFD model indicate that much CH_2O is formed at the end of LTR, i.e. 20°BTDC, and the distribution is rather uniform. However, at 20°BTDC little CH_2O resides in the piston-ring crevice region, because the CH_2O formation reactions are prohibited by the low temperature there. At the beginning of HTR, i.e. 10°BTDC, more CH_2O is formed in the combustion chamber core zone and squish region, because the temperature at the location is higher than the rest of the place. There are different levels of CH_2O concentration gradients near the cylinder head and the piston-ring crevice region because the formation of CH_2O is hindered by the heat transfer through those surfaces. At 9°BTDC, CH_2O almost fills the entire combustion chamber. At the end of HTR, i.e. 8°BTDC, the majority of CH_2O is consumed, and only a small portion of CH_2O resides in the piston-ring crevice region, where the CH_2O is most likely to appear.

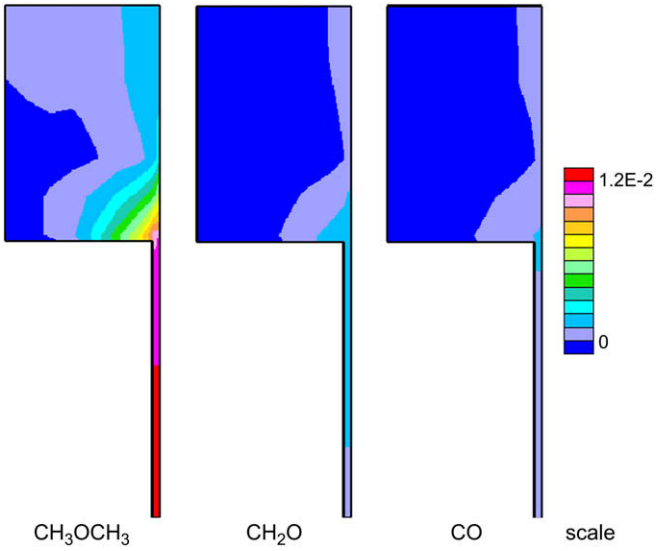

Fig. 13. The mass fraction distributions of major HC and CO emissions at EVO (the enlarged piston-ring crevice region) $\Phi_{DME} = 0.138$.

4.3. Analysis of emissions

The high level of unburned hydrocarbon and carbon monoxide emissions is a challenge for HCCI combustion. The percentage of fuel carbon into emissions is shown in Fig. 11 for $\Phi_{DME} = 0.138$. The efficiency for DME HCCI combustion process is rather high, and 96.85% of carbon in DME is converted into CO_2, and unburned hydrocarbon shares greater part than CO. Emission analysis indicates that unburned DME and CH_2O account for the majority of unburned hydrocarbon, and the unburned DME account for about 70% of HC, shown in Fig. 12.

The mass fraction distributions of major HC and CO emissions are shown in Fig. 13. Multi-dimensional CFD model indicates that the majority of HC is located in the piston-ring crevice region, and this region is amplified to obtain a clear view of the emission distributions.

During LTR only a small amount of DME is consumed in the upper part of piston-ring crevice region, but at the end of HTR the DME residing in the upper part almost disappears, leaving a large amount of DME in the bottom part of piston-ring crevice region, shown in Fig. 9. As piston moves downwards, some DME outflows from the piston-ring crevice region, as shown in Fig. 13. Unburned DME mainly resides in the bottom of piston-ring crevice region. The temperature in that region is the lowest because of the intense wall heat transfer, and LTR can hardly occur. A reduction of piston-ring crevice volume is an efficient way to reduce unburned DME emission.

During LTR only a small amount of CH_2O appears in the upper part of piston-ring crevice region, shown in Fig. 10. Until the end of HTR a certain amount of CH_2O is formed in the piston-ring crevice region. The heat released from the combustion chamber core zone heats the piston-ring crevice region. Thus, the reactions leading to the formation of CH_2O occur here. As piston moves downwards, some CH_2O outflows from the piston-ring crevice region, as shown in Fig. 13. A smaller amount of CH_2O is located in the upper part of the piston-ring crevice region than in the middle part, because the temperature is comparatively higher in the upper part of the piston-ring crevice region. Thus, much CH_2O is oxidized into CO in the upper part. However, a large amount of CH_2O resides in the middle of the piston-ring crevice region, because the temperature there is not high enough to initiate the oxidation of CH_2O-to-CO.

The CO-to-CO_2 reactions contribute significantly to the energy release during the HTR. The majority of CO resides in the upper part of piston-ring crevice region. The reason is that the temperature in the upper part is only sufficient to initiate oxidation of CH_2O-to-CO, but not high enough to initiate the CO-to-CO_2 reactions. Thus, much CO is left in the upper part of the piston-ring crevice region, shown in Fig. 13.

The effect of DME equivalence ratio on the conversion ratio of fuel carbon into emissions is shown in Fig. 14. As DME equivalence ratio decreases, unburned DME and CH_2O emissions increase, and CO emission increases. Thus, less fuel is converted into CO_2. When the DME equivalence ratio is too small, i.e. $\Phi_{DME} < 0.02$, the CO emission decreases rapidly, and the unburned DME and CH_2O emissions increase. The reason is that with the extremely lean fuel air mixture, the temperature in the combustion chamber is too low to initiate the low temperature reactions. The CO emission decreases, and much unburned DME is left in the combustion chamber.

5. Conclusions

1. Throughout the DME HCCI combustion process, the in-cylinder temperature distribution undergoes a process from inhomogeneity to homogeneity.
2. DME HCCI combustion process does not take place in the entire combustion chamber simultaneously. The low temperature reaction occurs primarily at the place near the piston surface and the squish region, and subsequently moves to the place near cylinder head. The high temperature reaction is initiated in the combustion chamber core zone and squish region, and then spreads to the rest of the combustion chamber.
3. Emission analysis indicates that unburned fuel and CH_2O account for the majority of HC emission. The unburned fuel, CH_2O and CO mainly resides in the bottom, middle and upper part of the piston-ring crevice region, respectively.
4. As the decrease of DME equivalence ratio, unburned fuel and CO increases. However, when the DME equivalence ratio is too small, the CO emission decreases.

Acknowledgments

The research is supported by the National Natural Science Foundation of China through its project (50376046) and by the Ministry of Science and Technology through its 973 National Key Project on HCCI Combustion Engines and Fuels (2001CB209201).

References

[1] T.A. Semelsberger, R.L. Borup, H.L. Greene, Dimethyl ether (DME) as an alternative fuel, J. Power Sources 156 (2006) 497–511.
[2] M. Sjböerg, J.E. Dec, An investigation into lowest acceptable combustion temperatures for hydrocarbon fuels in HCCI engines, Proc. Combust. Inst. 30 (2005) 2719–2726.
[3] S.C. Kong, R.D. Reitz, Numerical study of premixed HCCI engine combustion and its sensitivity to computational mesh and model uncertainties, Combust. Theor. Model 7 (2003) 417–433.
[4] J. Song, Z. Huang, X.Q. Qiao, W.L. Wang, Performance of a controllable premixed combustion engine fueled with dimethyl ether, Energy Convers. Manag. 45 (13–14) (2004) 2223–2232.
[5] C. Arcoumanis, C. Bae, R. Crookes, E. Kinoshita, The potential of di-methyl ether (DME) as an alternative fuel for compression-ignition engines: a review, Fuel (2007). doi:10.1016/j.fuel.2007.06.007.
[6] T. Shudo, Y. Ono, T. Takahashi, Ignition control by DME-reformed gas in HCCI combustion of DME, SAE Paper 2003-01-1824 (2003).
[7] T. Shudo, T. Takahashi, Influence of reformed gas composition on HCCI combustion of onboard methanol-reformed gases, SAE Paper 2004-01-1908 (2004).
[8] S. Sato, S.P. Kweon, D. Yamashita, N. Iida, Influence of the mixing ratio of double componential fuels on HCCI combustion, Int. J. Automot. Technol. 7 (3) (2006) 251–259.
[9] H. Yamada, M. Ohtomo, M. Yoshii, A. Tezaki, Controlling mechanism of ignition enhancing and suppressing additives in premixed compression ignition, Int. J. Engine Res. 6 (4) (2005) 331–340.
[10] D. Flowers, S. Aceves, C.K. Westbrook, J.R. Smith, R. Dibble, Detailed chemical kinetic simulation of natural gas HCCI combustion: gas composition effects and investigation of control strategies, J. Eng. Gas Turb. Power 123 (2) (2001) 433–439.
[11] M.F. Yao, Z.Q. Zheng, J. Qin, Experimental study on homogeneous charge compression ignition combustion with fuel of dimethyl ether and natural gas, J. Eng. Gas Turb. Power 128 (2) (2006) 414–420.
[12] M.F. Yao, Z. Chen, Z.Q. Zheng, B. Zhang, Y. Xing, Study on the controlling strategies of homogeneous charge compression ignition combustion with fuel of dimethyl ether and methanol, Fuel 85 (14–15) (2006) 2046–2056.
[13] S.C. Kong, A study of natural gas/DME combustion in HCCI engines using CFD with detailed chemical kinetics, Fuel 86 (2007) 1483–1489.
[14] R. Ogink, Computer modeling of HCCI combustion, Ph.D. thesis, Chalmers University of Technology, Sweden (2004).
[15] S.L. Fischer, F.L. Dryer, H.J. Curran, The reaction kinetics of dimethyl ether. I: high-temperature pyrolysis and oxidation in flow reactors, Int. J. Chem. Kinet. 32 (2000) 713–740.
[16] H.J. Curran, S.L. Fischer, F.L. Dryer, The reaction kinetics of dimethyl ether. II: low-temperature pyrolysis and oxidation in flow reactors, Int. J. Chem. Kinet. 32 (2000) 741–759.
[17] H. Yamada, Simplified oxidation mechanism of DME applicable for compression ignition, SAE Paper 2003-01-1819 (2003).
[18] H. Kim, S. Cho, K. Min, Reduced chemical kinetic model of DME for HCCI combustion, SAE Paper 2003-01-1822 (2003).
[19] M.F. Yao, J. Qin, Z.Q. Zheng, Numerical study of the combustion mechanism of a homogeneous charge compression ignition engine fuelled with dimethyl ether and methane, with a detailed kinetics model. Part 1: the reaction kinetics of dimethyl ether, Proc. I MechE Part D J. Aut. 219 (2005) 1213–1223.
[20] X. Liang, M.F. Yao, Z.Q. Zheng, Numerical study on the mechanism of low temperature reaction of DME/methanol HCCI combustion, J. Combust. Sci. Technol. 11 (2) (2005) 149–154 (in Chinese).
[21] S.M. Aceves, D.L. Flowers, C.K. Westbrook, J.R. Smith, W. Pitz, R. Dibble, M. Christensen, B. Johansson, A multi-zone model for prediction of HCCI combustion and emissions, SAE Paper 2000-01-0327 (2000).
[22] S.M. Aceves, D.L. Flowers, Spatial analysis of emissions sources for HCCI combustion at low loads using a multi-zone model, SAE Paper 2004-01-1910 (2004).
[23] A. Babajimopoulos, D.N. Assanis, D.L. Flowers, S.M. Aceves, R.P. Hessel, A fully integrated CFD and multi-zone model with detailed chemical kinetics for the simulation of PCCI engines, 15th International Multidimensional Engine Modeling User's Group Meeting. Detroit, MI, April (2005).
[24] L. Noel, F. Maroteaux, Numerical study of HCCI combustion in diesel engines using reduced chemical kinetics of n-heptane with multidimensinal CFD code, SAE Paper 2004-01-1909 (2004).
[25] M.F. Yao, C. Huang, Z.L. Zheng, Multidimensional numerical simulation on dimethyl ether/methanol dual-fuel homogeneous charge compression ignition (HCCI) engine combustion and emission processes, Energy Fuels 21 (2007) 812–821.
[26] CD adapco Group. STAR/Kinetics manual, Computational Dynamics Limited (2004).